Experimental Examination of Steel Bar Reinforcements on the Compressive Responses of Square CFST Short Columns

Ayce Cathen Winti[1], Abdul Azim Abdullah[1*], Abdul Razak Abdul Karim[1] and Ahmad Beng Hong Kueh[1,2]

[1] Department of Civil Engineering, Universiti Malaysia Sarawak, 94300 Kota Samarahan, Malaysia
[2] UNIMAS Water Centre (UWC), Universiti Malaysia Sarawak, 94300 Kota Samarahan, Malaysia

[*]E-mail: aaazim@unimas.my

Abstract. Square concrete-filled steel tube (CFST) columns offer construction efficiency but are significantly more prone to local buckling and possess lower confinement compared to circular sections. While various strengthening schemes exist, they often pose fabrication challenges or compromise steel tube integrity. This study investigates the mechanical behaviour of square CFST short columns reinforced with internal steel bars attached via a spot-welding technique, designed to minimize residual stress and simplify fabrication. Five specimens were tested under axial compression to evaluate the effects of varying steel bar diameters (10 mm and 12 mm) and quantities (4, 8 or 12 bars). The configuration used in this study also differs from those in previous studies. Experimental results indicate that the reinforced specimens achieved ultimate axial loads ranging from 559.4 kN to 839.2 kN, representing a significant capacity increase of 47% to 121% over the unreinforced specimen. Furthermore, the spot-welded reinforcement enhanced ductility by up to 103% and total energy absorption by up to 217%. The findings conclude that this spot-welded internal reinforcement method is an effective, construction-friendly solution for delaying local buckling and improving the overall compressive performance of square CFST columns.

Keywords: Square CFST, Short columns, Steel bar reinforcement, Compressive behaviour, Ductility

1. Introduction

Concrete-filled steel tubes (CFST) have gained popularity in structural engineering due to their superior strength, ductility, seismic performance and fire resistance resulting from the composite action between the concrete core and steel tube [1]. Additionally, the steel tube acts as permanent formwork, significantly reducing construction costs and time [2,3]. Despite the superior confinement of circular sections, square sections are increasingly favored for their practical advantages in simplifying beam-to-column joint fabrication [4,5]. However, square CFST columns

are prone to local buckling and exhibit reduced bearing capacity compared to circular counterparts, highlighting the need for effective strengthening solutions.

Recent research has explored various enhancement schemes, such as longitudinal plate stiffeners [6], binding bars [7], inclined stiffeners [8], rhombic stirrups [9] and semi-circular stiffeners [10]. Nevertheless, these strengthening schemes have their limitations. Installing such systems within small-sized steel tubes poses significant practical challenges and the drilling required for binding bars can induce stress concentrations, potentially compromising the structural integrity of the steel tubes. Furthermore, there is a distinct lack of studies utilizing internal bars attached via spot-welding as a primary reinforcement method.

To address these limitations, this study investigates square CFST short columns reinforced with internal steel bars attached via spot-welding. This technique offers a construction-friendly alternative that minimizes residual stress and fabrication time compared to existing methods. In order to evaluate the effectiveness and feasibility of this reinforcement method, axial loading tests were conducted to evaluate the influence of steel bar diameter and quantity on the compressive strength, ductility and energy absorption of the short columns.

2. Experimental test

2.1 General

This study experimentally investigated the axial compressive behaviour of square CFST short columns subjected to monotonic axial loading. A total of five specimens were categorised into three groups: Group A (unreinforced), Group B (varying steel bar reinforcement diameters) and Group C (different quantities of steel bar reinforcement). All columns were designed with a nominal height of 300 mm and a 100 mm × 100 mm cross-section, with a height-to-width ratio of three (3). This aspect ratio, prevalent in experimental programmes investigating CFST short column behaviour, ensures the prevailing failure mode reflects material response rather than global buckling [11–16]. The key geometric properties of the specimens are summarised in Figure 1. Specimens labelled with 'SB' represent specimen reinforced with internal steel bars, whereas 'UR' denotes unreinforced specimen. The numerical value indicates the quantity of steel bars and finally the diameter of the steel bars. Steel tube wall thickness was 1.9 mm for all specimens. Table 1 summarises the specimen details and key parameters for all column specimens.

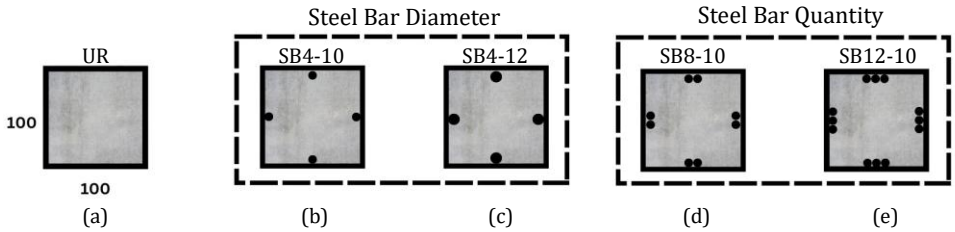

Figure 1. Cross-sectional configurations of the tested square CFST specimens: (a) Group A: unreinforced control specimen; (b)-(c) Group B: reinforced specimens with 10mm and 12mm diameter; (d)-(e) Group C: Specimens reinforced with 8 and 12 steel bars.

Table 1. Details of the specimens.

Specimen	B (mm)	H (mm)	t (mm)	⌀ (mm)	r (mm)	A_a (mm^2)	A_c (mm^2)	A_s (mm^2)
UR	100.0	100.0	1.9	-	3.0	735.6	9250.7	-
SB4-10	100.0	100.0	1.9	10.0	3.0	735.6	8936.5	314.2
SB4-12	100.0	100.0	1.9	12.0	3.0	735.6	8798.3	452.4
SB8-10	100.0	100.0	1.9	10.0	3.0	735.6	8622.3	628.3
SB12-10	100.0	100.0	1.9	10.0	3.0	735.6	8308.2	942.5

Note: B-Steel Tube Width; H-Steel Tube Height; t-Steel Tube Thickness; ⌀-Steel Bar Diameter; r-Inside Bend Radius of Steel Tube; A_a-Cross-Sectional Area of Steel Tube; A_c-Cross-Sectional Area of Concrete; A_s-Cross-Sectional Area of Steel Bar.

2.*2 Material testing*

The material properties of the steel tubes and steel bars are summarised in Table 2. The steel tubes utilised in this research were fabricated from mild steel. Tensile coupon tests were carried out in accordance with ISO 6892-1:2019 [17], using specimens machined from the flat faces of the steel tubes and representative sections of the steel bars. The test were carried out using the Hung Ta HT-2101 Electro-Hydraulic Servo Universal Testing Machines with a capacity of 300 kN.

Concrete cubes were tested on the 28 days with a concrete mix ratio of 1.00:0.47:1.36:2.53 (Cement: water: fine aggregate: coarse aggregate). With a water-cement ratio of 0.47, the mix was designed to provide sufficient workability for placement. Compressive strength of the concrete was assessed from three 150 mm cubes prepared from the same batch and cured under ambient laboratory conditions until the day of testing. The mean concrete cube strength (f_{cu}) recorded during testing was 26.0 MPa, with a standard deviation of 0.45 MPa.

2.3 *Test setup and loading*

The square CFST short column was reinforced with a steel bars that was attached to the inner surface of the steel tubes by using spot-welding techniques (Group B and C). The welds positions located around 25 mm from each edge to guarantee effective load transfer. Post-welding, specimens were inspected for weld integrity and alignment. Concrete placement was carried out in three successive layers by using a high-frequency poker vibrator to eliminate air voids from each layer for ensuring uniform density across the specimen. Prior to testing, the column ends were precision-ground using a rotary grinding wheel to ensure proper alignment with the testing

Table 2. Material properties of steel.

Type	t (mm)	⌀ (mm)	f_y (MPa)	f_u (MPa)	E (GPa)
Steel Tube	1.9	-	269.2	390.2	209.3
Steel Bar	-	10.0	515.6	608.9	190.8
Steel Bar	-	12.0	541.2	643.8	216.2

Note: t-Steel Tube Thickness; ⌀-Steel Bar Diameter; f_y-Yield Strength; f_u-Ultimate Strength; E-Young's Modulus

machine platens and eliminate surface irregularities that could compromise load distribution across the square CFST short column specimens' surfaces.

The axial compression tests were performed using a UTEST UTC-4730 compression machine with a loading capacity of 2000 kN. The load was applied incrementally using displacement control method at a constant rate of 1 mm/min until the post-peak load reached approximately 70% of the ultimate strength. The experimental setup shown in Figure 2, incorporated two linear variable displacement transducers (LVDTs) mounted symmetrically on the top loading platen to measure axial deformations. Displacement measurements of the specimens are captured in real time using LVDT transducers which connected to the Kyowa UCAM-60A data logger. All system components, including the load frame, servo-controller and data logger were connected to a dedicated local computer workstation.

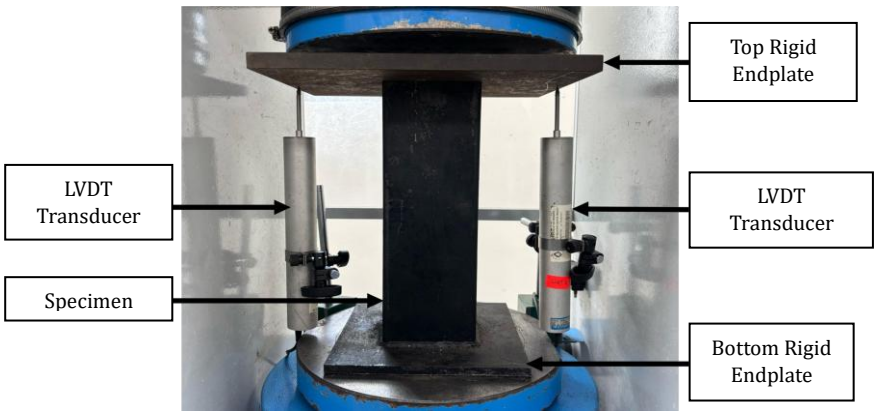

Figure 2. Test setup of the specimen.

3. Results and discussion

3.1 Failure mode

Figure 3 illustrates the failure modes observed in each specimen group under axial compression. For the unreinforced specimen (Group A), a distinct single outward local buckling wave developed at the mid-height of the steel tube. This classic buckling mode indicates substantial lateral expansion of the concrete core at the column's geometrically weakest point where end constraints are minimal.

Group B specimens displayed a transition in failure behaviour. Specimen SB4-10 exhibited a single mid-height buckling wave similar to the control. However, increasing the bar diameter in specimen SB4-12 resulted in a multi-wave pattern, where a primary local buckling at mid-height accompanied by a secondary local buckling wave near the top end, suggesting improved stress redistribution along the column height.

In contrast, Group C specimens (SB8-10 and SB12-10) demonstrated a distinct shift in failure location. The shift in local buckling location for Group C is attributed to the significant increase in lateral stiffness provided by the higher density of internal reinforcement (8 and 12 bars). While Group A and B specimens exhibited failure driven by the natural tendency of the column to bulge at its weakest unsupported length, which is the mid-height of the column, the closely spaced bars in Group C effectively restrained this expansion. Consequently, the critical failure zone shifted to the column ends, where stress concentrations are naturally higher due to the interaction with the rigid loading platens. Despite the crushing of the concrete core, all steel bar reinforced specimens exhibited ductile failure behaviour throughout the loading process.

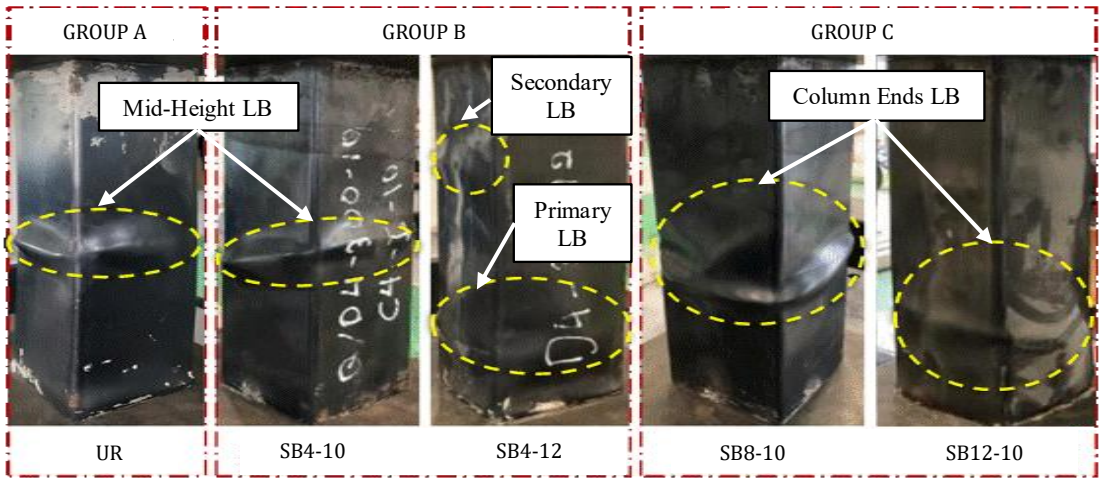

Figure 3. Failure mode of the specimens.

3.2 Axial load-shortening response

Figure 4 depicts the axial load-shortening response of the specimens under axial loading. All specimens exhibit an initial linear elastic response, where the applied load increases almost proportionally with axial shortening until yielding initiates. The stiffness of the specimens can be observed in this stage, as some of the specimens show slight steeper initial slope indicating early high resistance to deformation and a high degree of composite action. After reaching their respective peak load capacity (N_{ue}), the columns showed gradual strength reduction as progressive failure mechanisms developed under continued loading.

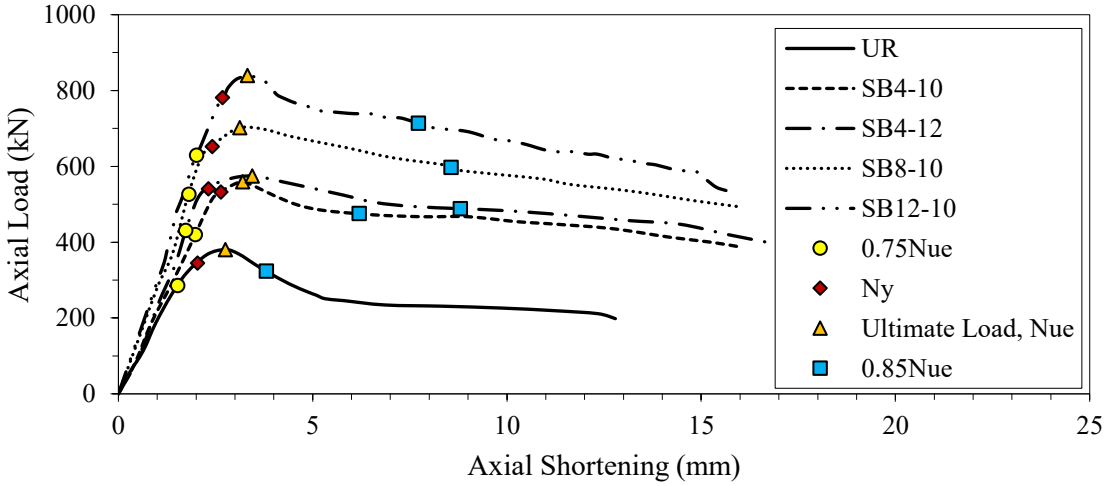

Figure 4. The axial load-shortening response characteristics of the specimens.

In particular, the UR specimen achieves a much lower peak load than the reinforced specimens. It clearly indicates the significant effect of using steel bars as reinforcement in reinforced specimens in terms of overall mechanical behaviour. Among these, the specimens with a higher quantity of steel bars reinforcement, which correspond to larger steel bar reinforcement area, appear to sustain greater loads before failure. This strongly indicates that the use of steel bars as reinforcement improves the axial load bearing capacity, likely due to better confinement

effects, which delay local buckling and improve the composite interaction between the steel tube and the concrete core.

3.3 Ultimate load

This section assesses the influence of steel bar reinforcement on the ultimate axial load capacity of square CFST short columns. The strength enhancement attributable to steel bars is quantified using the ultimate axial load enhancement index (UEI), defined as:

$$\mathrm{UEI} = \frac{N_{\mathrm{ue,sk}}}{N_{\mathrm{ue,0}}} \tag{1}$$

where $N_{\mathrm{ue,sk}}$ and $N_{\mathrm{ue,0}}$ denote the ultimate axial load of square CFST short columns with steel bar and unreinforced specimens, respectively.

To assess the role of steel bar as reinforcement in the square CFST short column specimens, the strength index (SI) is commonly used [18]. This dimensionless parameter is defined as:

$$\mathrm{SI} = \frac{N_{\mathrm{ue}}}{A_{\mathrm{a}}f_{\mathrm{y}}+A_{\mathrm{c}}f_{\mathrm{c}}'+A_{\mathrm{s}}f_{\mathrm{y,sk}}} \tag{2}$$

The denominator in Equation 2 represents the composite cross-section capacity. Within this equation, A_{a}, A_{c} and A_{s} denote the cross-sectional areas (mm^2) of the steel tube, infilled concrete core and steel bar, respectively. The yield strengths of the steel tube (f_{y}) and steel bar ($f_{\mathrm{y,sk}}$) are expressed in $\mathrm{N/mm}^2$. The characteristic cylinder compressive strength (f_{c}') is determined following Equation 3 as proposed in [19].

$$f_{\mathrm{c}}' = f_{\mathrm{cu}}[0.76 + 0.2\log_{10}\left(\frac{f_{\mathrm{cu}}}{19.6}\right) \tag{3}$$

where f_{cu} is the average cube compressive strength of concrete stated in Section 2.2.

Table 3 highlights the significant difference in axial load-bearing capacity between the unreinforced and reinforced columns. The unreinforced specimen (UR) exhibited the lowest ultimate axial load of 380.5 kN. The introduction of steel bars consistently improved capacity, directly correlating with both increased bar diameter and quantity. For instance, increasing the bar diameter from 10 mm (SB4-10) to 12 mm (SB4-12) resulted in a capacity increase from 559.4 kN to 574.7 kN, as shown in Figure 5(a).

The impact of reinforcement quantity was even more pronounced. Specimen SB8-10 (8 bars) achieved 702.2 kN, while SB12-10 (12 bars) reached the maximum observed load of 839.2 kN, as shown in Figure 5(b) This enhancement is attributed to the improved confinement effects provided by the steel bars, which delay local buckling and distribute axial loads more efficiently across the composite section.

Overall, the internal spot-welded reinforcement resulted in a substantial ultimate load enhancement index (UEI) compared to the unreinforced baseline. While increasing the steel bar diameter resulted in a modest average improvement of approximately 47%, increasing the quantity of bars proved more effective, culminating in a 121% capacity increase for the specimen with 12 reinforcing bars (SB12-10). The mean SI ratio across the specimens was 0.99, while the coefficient of variation (CoV) for this ratio was 0.04, reflecting a low level of dispersion and good consistency across the tested reinforced specimens. It also means that the axial load bearing capacity can be accurately predicted by the composite cross-section capacity method.

Table 3. Overview of experimental findings.

Specimen	Ultimate axial strength				Ductility		Energy absorption		
	N_{ue} (kN)	N_y (kN)	SI	UEI	DI	DEI	EA_{pre} (kN·mm)	EA_{post} (kN·mm)	EA_t (kN·mm)
UR	380.5	345.2	1.00	1.00	1.87	1.00	647.6	2507.0	3154.6
SB4-10	559.4	532.1	1.04	1.47	2.35	1.26	1042.8	5833.1	6875.9
SB4-12	574.7	540.5	0.93	1.51	3.79	2.03	1264.8	6397.9	7662.8
SB8-10	702.2	652.4	1.01	1.85	3.56	1.90	1303.2	7563.8	8867.0
SB12-10	839.2	781.0	0.99	2.21	2.88	1.54	1624.2	8378.1	10002.3
Mean			0.99						
CoV			0.04						

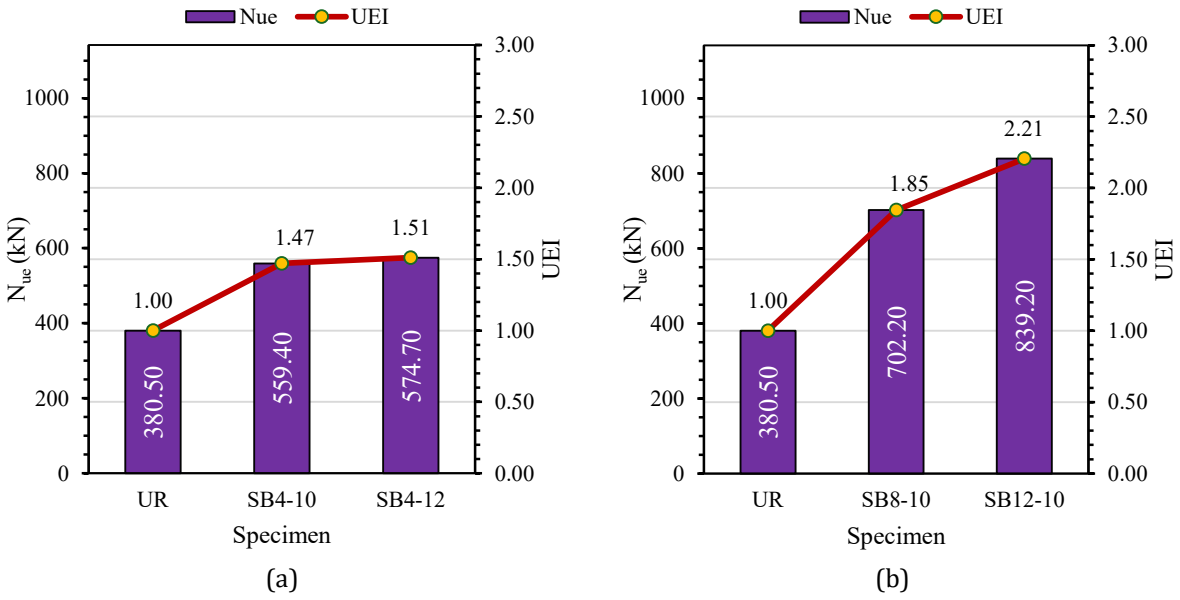

Figure 5. Influence of steel bar parameters on ultimate axial load: (a) Diameter; (b) Quantity.

3.4 Ductility

Ductility refers to a structure's capacity to withstand inelastic deformation before collapsing, without experiencing a substantial reduction in strength. A highly ductile structure can effectively redistribute stress and exhibit increasing deflections, serving as a warning sign before collapse. To assess the influence of using steel bars reinforcement on specimens' ductility, this study utilises the ductility index (DI), a measure adopted by previous researcher [20]. The equation for DI can be defined as:

$$\mathrm{DI} = \frac{\Delta_u}{\Delta_y} \tag{4}$$

where Δ_u represents the displacement at which the applied load reduces to 85% of its peak value during the descending phase of the load-shortening curve. Meanwhile, Δ_y is established using the secant stiffness, defined by a straight line connecting the origin to the point where the load reaches 75% of its peak value. The load value at this intersection defines the yield load, N_y, which is as shown in Figure 6.

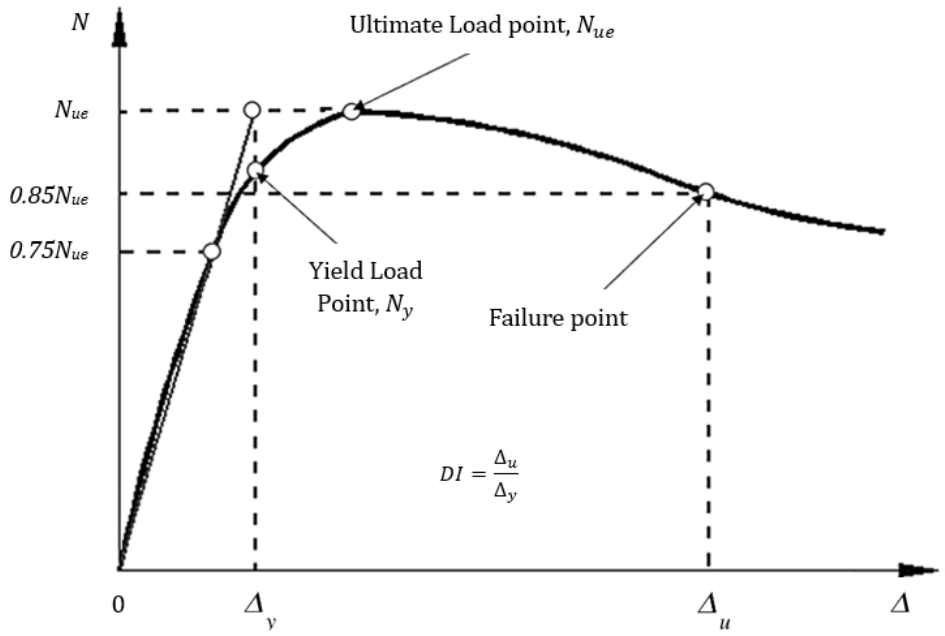

Figure 6. Definition of ductility index [21].

In order to quantify the improvement of ductility of specimens with the application of steel bars as reinforcement, the ductility enhancement index (DEI) was employed in this study. It was calculated as the ratio of the ductility of reinforced specimens to that of unreinforced specimens, as expressed in equation below:

$$\text{DEI} = \frac{DI_{\text{SB}}}{DI_0} \tag{5}$$

where DI_{SB} represents the ductility index of the specimen with steel bars as reinforcements, while DI_0 refers to the ductility index of the unreinforced specimen. The ductility of the square CFST short column specimens is presented in Table 3.

Table 3 presents a comparison of the DI and DEI for the tested specimens, highlighting the influence of steel bar reinforcement on ductility performance. The unreinforced column (UR) has the smallest DI of 1.87, which serve as the critical baseline for comparison. This indicates a limited ability of unreinforced specimen to undergo deformation before failure in comparison to the reinforced specimens, which align with the specimen ultimate axial load.

In contrast to the unreinforced specimen, reinforced specimens demonstrated a better improvement in both the strength and deformability. Specimens with larger diameter of steel bars such as the SB4-12, achieved a DI of 3.79 and DEI of 2.03, which is an improvement of 62% compared to SB4-10 with a DI of 2.35 and DEI of 1.26, as shown in Figure 7(a). The larger diameter of steel bar able to improve the ductility of the specimens up to 103% in comparison to unreinforced specimens. The axial load-shortening curve as shown in Figure 4 further corroborates this enhancement, displaying an extended deformation plateau attributed to the improved stress distribution, delayed local buckling and the enhanced concrete lateral

deformation. These results further suggest that larger steel bar diameters enhance the composite action, which enable more uniform stress distribution prior to failure.

Increasing the reinforcement quantity revealed that ductility does not increase linearly with strength. While specimen SB12-10 achieved the highest ultimate axial load, its DI was 19% lower than that of specimen SB8-10, as shown in Figure 7(b). This reduction highlights the competing effects of confinement and axial stiffness. While the dense arrangement of 12 steel bars provides substantial confinement, it also significantly increases the axial stiffness of the composite section. This excessive stiffness rigidly restricts the lateral dilation of the concrete core, preventing the gradual plastic deformation observed in moderately reinforced specimens. This demonstrated that an optimal balance between confinement and stiffness is required to maximize ductility.

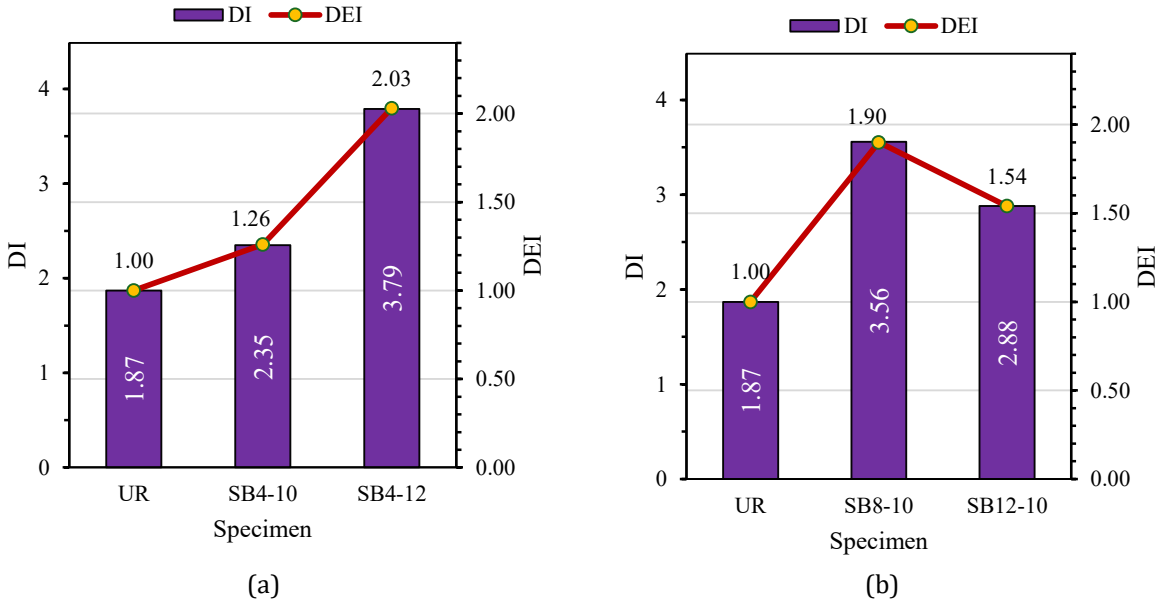

Figure 7. Influence of steel bar parameters on ductility: (a) Diameter; (b) Quantity.

3.5 Energy absorption

Energy absorption is typically calculated by determining the area under the axial load-shortening curve derived from the continuous displacement-controlled loading method. The curve was divided into pre-peak and post-peak segments to assess the effects of steel bar reinforcements on column toughness. Pre-peak energy (EA_{pre}) was measured up to the ultimate axial load (N_{ue}), post-peak energy (EA_{post}) was calculated beyond this point until testing ceased at 70% residual strength and the total energy absorption (EA_{t}) was the sum of EA_{pre} and EA_{post}. The calculated energy absorption capacities for all specimens are presented in Table 3.

UR attains the smallest total energy absorption, demonstrating limited energy absorption capacity. This shows the very strong beneficial effect of steel bar reinforcement on energy absorption. Reinforced specimens exhibited 118–217% greater EA_{t} compared to the unreinforced specimen, as shown in Figure 8.

This substantial increase, particularly in the post-peak phase (EA_{post}) is attributed to the bridging action of the steel bars. Even after the concrete core begins to crush, the internal bars maintain the composite integrity of the section and restrain the steel tube from rapid outward buckling, allowing the column to sustain significant residual loads during large inelastic deformations. From a design perspective, this enhanced energy dissipation capability suggests

that spot-welded internal reinforcement is particularly advantageous for structural components requiring high seismic ductility or blast resistance, where maintaining integrity beyond peak load is critical.

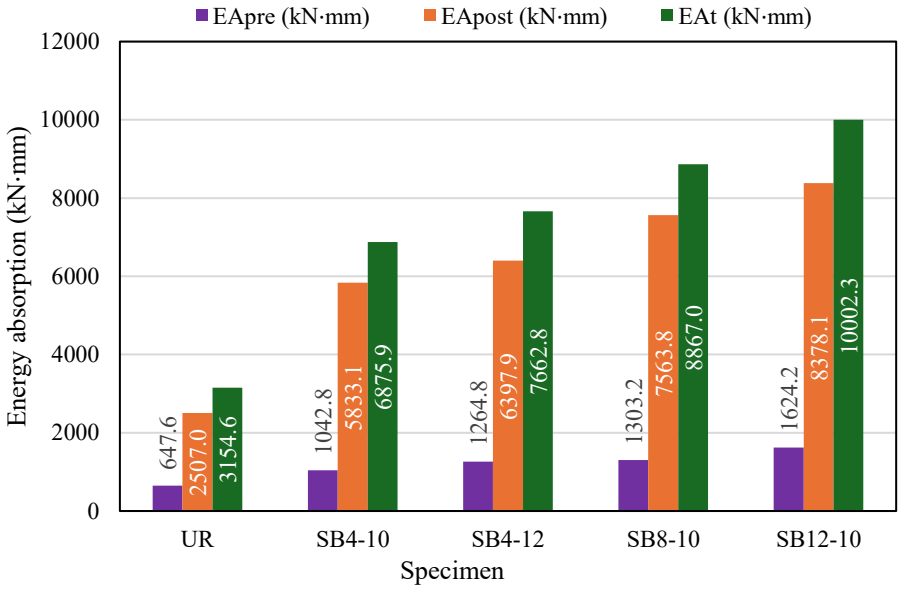

Figure 8. Effect of steel bar on energy absorption capacities of specimens.

4. Conclusion

This study experimentally investigated the structural behaviour of square CFST short columns reinforced with internal steel bars under axial compression, demonstrating that the proposed spot-welded reinforcement technique is able to enhance the performance of the specimens. Specifically, the reinforced specimens achieved an ultimate axial load capacity increase of 47% to 121% compared to unreinforced columns, effectively mitigating confinement lag and delaying local buckling. In addition to strength, the reinforcement substantially improved ductility by up to 103% and total energy absorption by up to 217%, suggesting that this method is highly suitable for structures in seismic zones or applications requiring high impact resistance where energy dissipation is critical. From a design perspective, the study confirms that internal spot-welding offers a construction-friendly alternative to complex external stiffeners. However, results indicate that excessive reinforcement can lead to stiffness-induced ductility reduction, necessitating an optimal balance between confinement and stiffness. Finally, as the scope of this work was limited to short columns subjected to monotonic axial loading, future research should investigate slender columns, eccentric loading conditions and cyclic loading behaviors to ensure reliability under diverse operational stresses.

Acknowledgments

The authors acknowledged the financial support from the Kementerian Pengajian Tinggi Malaysia, *Fundamental Research Grant Scheme* (*FRGS*), FRGS/1/2023/TK06/UNIMAS/02/1.

References

[1] Alatshan F, Osman S A, Hamid R and Mashiri F 2020 Stiffened concrete-filled steel tubes: A systematic review *Thin-Walled Structures* 148 106590
[2] Wang X, Fan F and Lai J 2022 Strength behavior of circular concrete-filled steel tube stub columns under axial compression: A review *Constr Build Mater* 322 126144
[3] Liang Z, Zheng S, Du Y and Song Z 2025 Seismic performance of CFST segmented composite lattice columns: Experimental and numerical simulation study *Constr Build Mater* 492 142877
[4] Hassanein M F, Kharoob O F and Gardner L 2015 Behaviour and design of square concrete-filled double skin tubular columns with inner circular tubes *Eng Struct* 100 410–24
[5] Klongaksornkul P and Phuvoravan K 2021 Experimental Investigation on Concrete Filled Steel Tube Columns under Concentric and Eccentric Loading *Civil Engineering and Architecture* 9 2397–415
[6] Tao Z, Han L-H and Wang Z-B 2005 Experimental behaviour of stiffened concrete-filled thin-walled hollow steel structural (HSS) stub columns *J Constr Steel Res* 61 962–83
[7] Cai J and He Z-Q 2006 Axial load behavior of square CFT stub column with binding bars *J Constr Steel Res* 62 472–83
[8] Liang W, Dong J F, Yuan S C and Wang Q Y 2017 Behavior of Self-Compacting Concrete-Filled Steel Tube Columns with Inclined Stiffener Ribs Under Axial Compression *Strength of Materials* 49 125–32
[9] Chen Z, Ning F and Mo L 2021 Experimental Study and Mechanism Analysis of Concrete-Filled Square Steel Tubular Columns Reinforced by Rhombic Stirrups Under Axial Compression *Front Mater* 8
[10] Li S, Liu F, Chan T-M, Yang H and Young B 2025 Novel concrete-filled steel square tubular columns stiffened with semi-circles: Concept and behaviour *Thin-Walled Structures* 212 113188
[11] Ci J, Kong L, Ahmed M, Liang Q Q, Hamoda A, Chen S and Wu C 2022 Experimental and numerical studies of axially loaded square concrete-encased concrete-filled large-diameter steel tubular short columns *Structural Concrete* 23 2748–69
[12] Tao Z, Han L-H and Zhao X-L 2004 Behaviour of concrete-filled double skin (CHS inner and CHS outer) steel tubular stub columns and beam-columns *J Constr Steel Res* 60 1129–58
[13] Wang Y, Chen J and Geng Y 2015 Testing and analysis of axially loaded normal-strength recycled aggregate concrete filled steel tubular stub columns *Eng Struct* 86 192–212
[14] Zhu A, Zhang X, Zhu H, Zhu J and Lu Y 2017 Experimental study of concrete filled cold-formed steel tubular stub columns *J Constr Steel Res* 134 17–27
[15] Zhou X, Zhou Z and Gan D 2020 Analysis and design of axially loaded square CFST columns with diagonal ribs *J Constr Steel Res* 167 105848
[16] Alatshan F, Osman S A, Altlomate A, Alkair M, Hamid R and Mashiri F 2023 Design Model of Rectangular Concrete-Filled Steel Tubular Stub Columns under Axial Compression *Buildings* 13
[17] International Organization for Standardization 2019 ISO 6892-1:2019: Metallic materials - Tensile testing - Part 1: Method of test at room temperature
[18] Tao Z, Han L H and Wang D Y 2008 Strength and ductility of stiffened thin-walled hollow steel structural stub columns filled with concrete *Thin-Walled Structures* 46 1113–28
[19] Mirza S A and Lacroix E A 2004 Comparative Strength Analyses of Concrete-Encased Steel Composite Columns *Journal of Structural Engineering* 130 1941–53
[20] Yu C Q, Tong G S, Tong J Z, Zhang J W, Li X G and Xu S L 2024 Experimental and numerical study on seismic performance of L-shaped multi-cellular CFST frames *J Constr Steel Res* 213
[21] Zhao P, Huang Y, Lu Y, Liang H and Zhu T 2022 Eccentric behaviour of square CFST columns strengthened using square steel tube and high-performance concrete jackets *Eng Struct* 253 113772